LETTERS
PUBLISHED ONLINE: 31 JULY 2011 | DOI: 10.1038/NNANO.2011.110
nature nanotechnology

Direct laser writing of micro-supercapacitors on hydrated graphite oxide films

Wei Gao[1], Neelam Singh[2], Li Song[2], Zheng Liu[2], Arava Leela Mohana Reddy[2], Lijie Ci[2], Robert Vajtai[2], Qing Zhang[3], Bingqing Wei[3] and Pulickel M. Ajayan[1,2]*

Microscale supercapacitors provide an important complement to batteries in a variety of applications, including portable electronics. Although they can be manufactured using a number of printing and lithography techniques[1–3], continued improvements in cost, scalability and form factor are required to realize their full potential. Here, we demonstrate the scalable fabrication of a new type of all-carbon, monolithic supercapacitor by laser reduction and patterning of graphite oxide films. We pattern both in-plane and conventional electrodes consisting of reduced graphite oxide with micrometre resolution, between which graphite oxide serves as a solid electrolyte[4–9]. The substantial amounts of trapped water in the graphite oxide makes it simultaneously a good ionic conductor and an electrical insulator, allowing it to serve as both an electrolyte and an electrode separator with ion transport characteristics similar to that observed for Nafion membranes[10,11]. The resulting micro-supercapacitor devices show good cyclic stability, and energy storage capacities comparable to existing thin-film supercapacitors[1].

Graphite oxide (GO) has recently attracted a great deal of attention, because it offers a low-cost, scalable and wet-chemical approach to graphene[12–16]. The conductivity of GO, which is dominated by ionic conductivity, depends on the environment and varies between 5×10^{-6} S cm^{-1} and 4×10^{-3} S cm^{-1} (refs 8 and 17), suggesting that GO is close to being electrically insulating. Here, we demonstrate that hydrated GO offers very interesting applications in energy storage devices when water is entrapped during processing or is absorbed following exposure to the environment or moisture. When a substantial amount of water is entrapped in the layered GO structure[9], it becomes a strongly anisotropic ionic conductor as well as an electrical insulator, enabling its use as a viable electrolyte and electrode separator. The ability to laser-reduce GO into conducting reduced graphite oxide (RGO) allows the facile and non-toxic writing of RGO–GO–RGO patterns in various configurations to build electrical double-layer capacitors (EDLC) or supercapacitors.

Recent reports[18,19] describe the laser reduction conversion of GO into RGO with different levels of reduction and various electrical conductivity improvements. It is possible to pattern any GO surface into RGO–GO–RGO structures in various geometries with micrometre resolution. We constructed both in-plane and conventional sandwich supercapacitor designs, in a number of patterns and shapes as described in Fig. 1 and Supplementary Fig. S1. All the proposed configurations of supercapacitor, conventional sandwich-like configuration and novel in-plane configurations can be directly built on a single piece of GO paper. The as-prepared laser-patterned devices (RGO–GO–RGO) demonstrate good electrochemical performance without the use of an external electrolyte (Fig. 2). Because of uncertainty in the measurement of the exact mass of the laser-reduced active electrode material, we will mainly report the capacitance values in area and volume density units. The measured capacitance seems to depend on the geometry of the design, as the ionic mobilities and transport distances (thickness of the separator section) are anisotropic and differ for different geometries. The in-plane supercapacitor structure with a circular geometry gives the highest capacitance (0.51 mF cm^{-2}), nearly twice that of the sandwich structure (Fig. 2a). A control experiment was carried out with pristine hydrated GO films and current collectors (with no reduced RGO part), and no capacitance was detectable. The equivalent series resistance (ESR) values obtained from the impedance spectra offer information about how fast the cells are charged/discharged. The in-plane structure has a higher ESR value than the sandwich structure (6.5 kΩ versus 126 Ω; Fig. 2b), indicating it has a lower charge/discharge rate (Supplementary Fig. S2a,b). A recently reported well-designed, inkjet-printed carbon supercapacitor with interdigitated electrode structure and similar electrode thickness had a mean capacitance density of 0.4 mF cm^{-2} with an organic electrolyte[18], showing that the performance of our device, without an external electrolyte, is in the same range as reported for other systems. For electrochemical double-layer microcapacitors, typical capacitance values reported in the literature fall between ~0.4 and 2 mF cm^{-2} (ref. 3).

The ionic conductivity of hydrated GO was calculated from the impedance spectra obtained for the devices (see Methods for details)[20], giving values of 1.1×10^{-5} S cm^{-1} for the sandwich geometry and 2.8×10^{-3} S cm^{-1} for the in-plane one. This anisotropy can be easily explained by the microscopic GO sheet arrangement shown in Supplementary Fig. S2. The hydrated GO film has an anisotropic structure with a *z*-lattice distance of 0.86 nm (obtained by means of X-ray diffraction (XRD) characterization; Supplementary Fig. S3), so ions can move more easily along the intralayer direction rather than normal to the layers. This is similar to the anisotropic electrical conductivity reported for graphite and GO platelets[21].

In EDLCs, electrical energy storage is achieved by nanoscopic charge (ion) separation at the interface between the electrode and electrolyte. In our system, the only source of ions is the hydrated GO. The morphology and structure of a GO film is shown in Supplementary Figs S4b and S2c. The higher value of the interlayer spacing (0.86 nm, Supplementary Fig. S3) in hydrated GO than in completely dehydrated GO (reported to be 0.567 nm in ref. 9) is an indication of the high water content within our films. We have characterized the water content in hydrated GO to be ~16 wt% by means of Karl–Fischer titration[8]. The interaction between the trapped water and GO layers is key to the ionic conductivity observed here. At low concentration, H_2O molecules bind to GO sheets through a strong intermolecular interaction (hydrogen

[1]Department of Chemistry, Rice University, Houston, Texas 77005, USA, [2]Mechanical Engineering and Materials Science Department, Rice University, Houston, Texas 77005, USA, [3]Department of Mechanical Engineering, University of Delaware, Newark, Delaware 19716, USA. *e-mail: ajayan@rice.edu

© 2011 Macmillan Publishers Limited. All rights reserved.

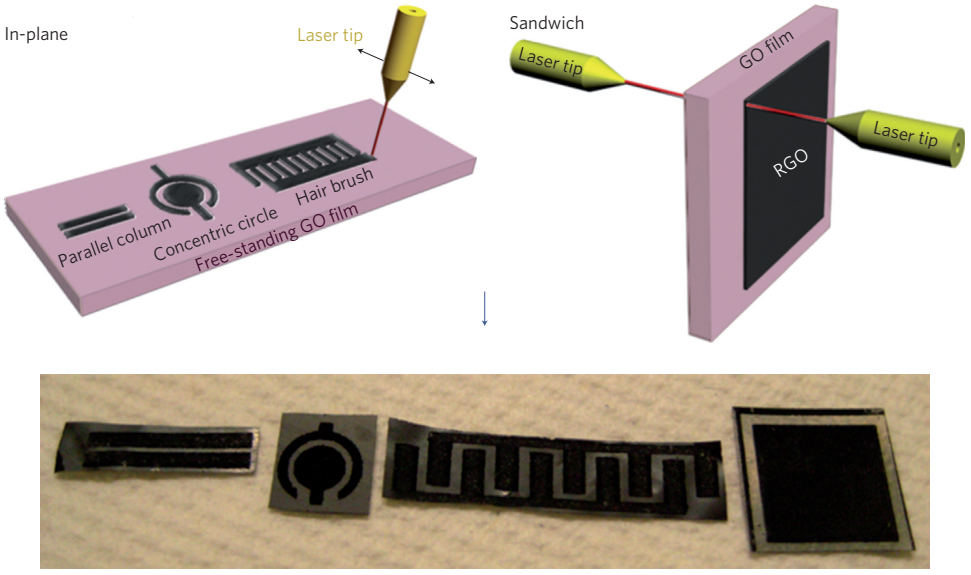

Figure 1 | Schematics of CO_2 laser-patterning of free-standing hydrated GO films to fabricate RGO–GO–RGO devices with in-plane and sandwich geometries. The black contrast in the top schematics corresponds to RGO, and the light contrast to unmodified hydrated GO. For in-plane devices, three different geometries were used, and the concentric circular pattern gives the highest capacitance density. The bottom row shows photographs of patterned films. Typical dimensions of these devices are mentioned in the caption to Supplementary Fig. S1.

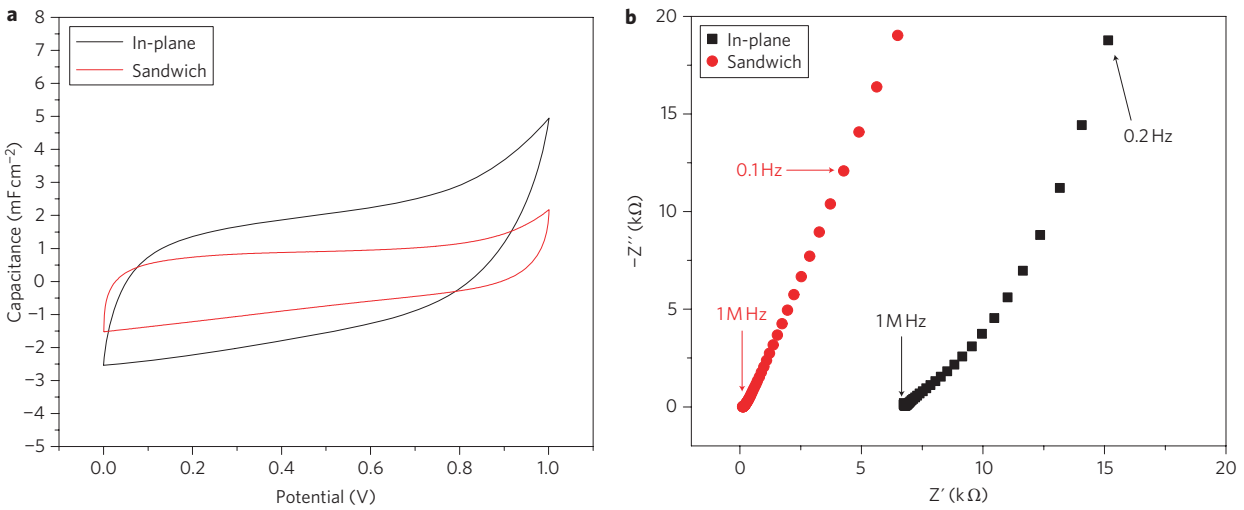

Figure 2 | Comparisons of CV and impedance behaviour of in-plane and sandwich devices. a, CV curves of in-plane circular and sandwich devices at a scan rate of 40 mV s^{-1}. The in-plane circular structure gives a specific capacitance twice that of the sandwich structure. **b**, Impedance spectra from 1 MHz to 10 mHz at 10 mV sinusoidal signal, zoomed in at the high-frequency region, demonstrating a much higher ESR value (the intercept of the slanted straight line with the Z′ axis) for the in-plane device than for the sandwich device, leading to a lower power density for the in-plane device. Z′, real part of impedance; Z″, imaginary part of impedance.

bonding). As the water content increases, the active sites on the GO sheets become saturated, and excess water molecules are free to rotate and diffuse. The water content at the reported transition point between the bonded-water and free-water states is ~15 wt% (ref. 9). We speculate that protons, which are the species taking part in ionic conduction, arise from hydrolysis of the functional groups (carboxyl, sulphonic[22] and/or hydroxyl) present on GO. The resulting protons are able to move by means of the Grotthuss mechanism[23] (hopping via the hydrogen-bonding network), or even migrate freely in the hydronium form (H_3O^+) within the intra-layer spaces (Supplementary Fig.S2). This proton transport seems to be similar to that observed in Nafion, a well-investigated polymer system that demonstrates water-induced proton transport following a hopping mechanism[24].

To study the dehydration–rehydration influence on pristine hydrated GO films, impedance spectroscopy measurements were conducted on the films (see Methods) while controlling the environment (under vacuum and at various humidity levels). A stepwise decrease in ionic conductivity (Fig. 3a) is observed with increasing exposure time to vacuum, and a full recovery is seen after re-exposure to air for 3 h. The ionic conductivity calculated from the impedance spectra versus exposure time plot is shown in Fig. 3b. After 6 h under vacuum, there is a two orders of magnitude decrease in the ionic conductivity of the device, which is also fully recovered after exposure to air, indicating the reversibility of this process at room temperature. To study the effect of moisture on the ionic conductivity of GO, impedance spectra measurements were conducted for the GO film at various humidity levels

© 2011 Macmillan Publishers Limited. All rights reserved.

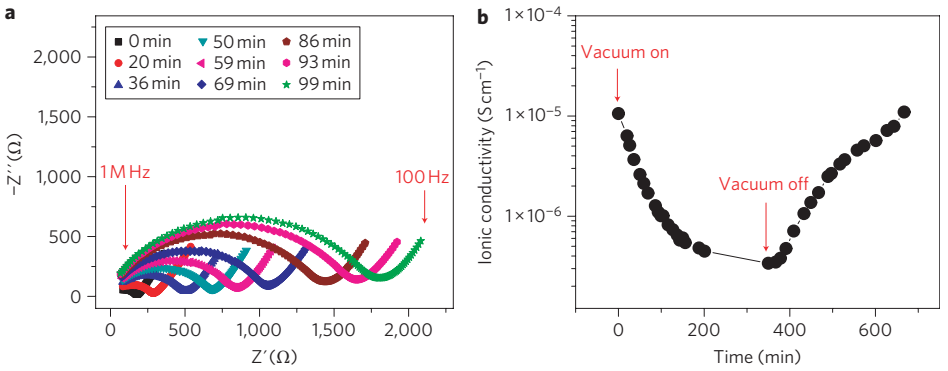

Chemical composition	Density	Water content	Colour	Ionic conductivity (from impedance spectroscopy)
$C_{3.9}O_{2.5}H_{0.9}$	1.1 g cm^3	16 wt%	Yellowish-brown	1.1×10^{-5} S cm^{-1} to 2.8×10^{-3} S cm^{-1}

Figure 3 | Characterization of the water effect on GO ionic conductivity. a, Stepwise change in impedance spectra versus exposure time to vacuum (0.08 MPa) at 25 °C. Cell structure: a pristine GO film coated with silver on both sides, and sandwiched between two pieces of stainless steel foil (1 cm × 1.2 cm); frequency range, 1 MHz to 100 Hz at 10 mV sinusoidal signal. Water is slowly evaporated out of the film under vacuum, leading to an increase in the arc diameter in the high-frequency range, which indicates a decrease in ionic conductivity. **b**, Dependence of ionic conductivity on exposure time to vacuum and air. Conductivity data were obtained from Z view fitting of the impedance spectra. The hydrated GO film became less conductive under vacuum, but recovered its full conductivity after 3 h of re-exposure to air. Four-probe electrical measurement on a single piece of pristine GO film also showed at least three orders of magnitude decrease in conductance under vacuum (Supplementary methods), indicating that in GO the major contribution to measured conductivity is ionic. **c**, Schematic of GO chemical structure, and table of measured physical properties of GO in an ambient environment. A sandwich geometry with well-defined cross-sectional area offered an accurate conductivity value of 1.1×10^{-5} S cm^{-1}, and the in-plane structure with an estimated cross-sectional area showed a higher ionic conductivity of 2.8×10^{-3} S cm^{-1}. We believe, due to the lamella structure of GO, its ionic conductivity is anisotropic. Upon hydration, the ionic conductivity further increases (Supplementary Fig. S4a,b), and becomes comparable to Nafion[10].

(Supplementary Fig. S4a,b). Almost three orders of change in magnitude of ionic conductivity was observed following hydration of the GO film (Supplementary Fig. S4b). The dramatic changes in ionic conductivity resemble the proton-conducting behavior of Nafion[24]. The chemical structure and properties of GO and Nafion are shown in Fig. 3c and Supplementary Fig. S4, respectively. The active group in Nafion is a sulphonic acid group[25], but in GO it could be a carboxylic acid group, a sulphonic acid group[22] or even a tertiary alcohol group. Furthermore, the large number of existing epoxy groups in GO could help proton migration. The application of Nafion as an electrolyte and separator in supercapacitor devices has been reported[11]. Our observations in relation to the Nafion-like conduction of hydrated GO strongly suggest that it is acting like an ionic conductor, with its ionic/proton conductivity influenced by the water content.

The fact that GO can be easily converted to RGO by means of laser radiation enables any number of in-plane or sandwiched RGO–GO–RGO supercapacitor devices to be produced in a scalable and simple manner via laser-patterning of hydrated GO. The active electrode material RGO, formed from hydrated GO using laser heating, is porous due to the gases produced from the decomposition of the functional groups[8] and water under localized laser heating (Fig. 4b, Supplementary Fig. S1). The dependence of RGO resistivity and reduction depth on laser power is shown in Supplementary Fig. S5, with a decrease in resistivity by up to four orders of magnitude achieved by this laser treatment, which is consistent with previously reported work[18]. The long-range ordered structure[26] in RGO (Fig. 4b) facilitates ion diffusion within the electrode. However, the short-range random arrangement of RGO flakes could lead to resistance to ion migration[27], as indicated in the impedance spectra (Fig. 2b). The cyclic stability tests performed on the supercapacitor devices are shown in Fig. 4c. After 10,000 cycles, there is an ~30% drop in the capacitance of the in-plane circular device, whereas an ~35% drop is observed for the sandwich devices. The drop in capacitance seen upon cycling is typical of many supercapacitor devices reported in literature[28,29]. This decline could be due to water loss in the device. Interestingly, the capacitance doubled when the same device, after long cycling, was kept in ambient conditions for a week (Supplementary Fig. S6).

The in-plane circular design shows the highest specific capacitance of ~0.51 mF cm^{-2}. Considering only the active thickness of the electrodes, the volumetric capacitance is ~3.1 F cm^{-3}, with the electrode volume estimated from the thickness of the reduced region (Supplementary Fig. S7). The energy density for this device is calculated to be ~4.3×10^{-4} W h cm^{-3}, with a power density of 1.7 W cm^{-3}. Owing to its lower ESR value, the sandwich device geometry gives a higher power density of ~9.4 W cm^{-3}, although the energy density for this device is lower (1.9×10^{-4} W h cm^{-3}). A good match between the 20 mV s^{-1} and 40 mV s^{-1} cyclic voltammetry (CV) scan rates (Supplementary Fig. S8) suggests similar ion diffusion paths within this range of scan rates[30]. However, we did observe a decrease in capacitance when the scan rate was increased to 100 mV s^{-1}. This could be due to the inhomogeneous pore structure within the electrodes or the pseudo-capacitance caused by

© 2011 Macmillan Publishers Limited. All rights reserved.

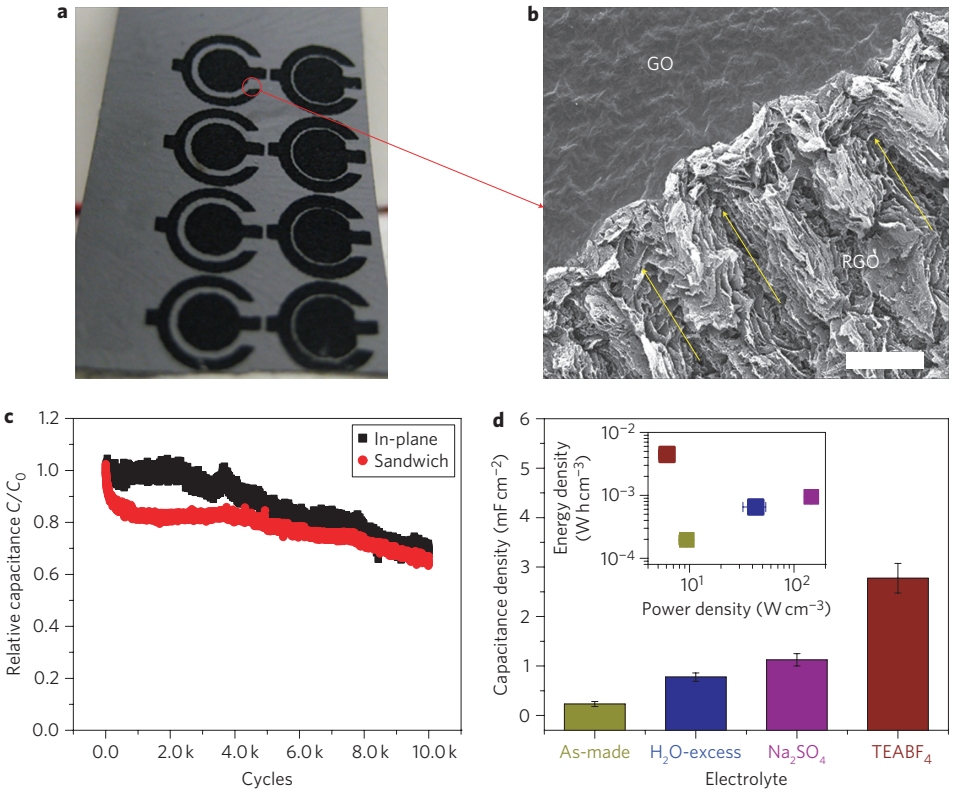

Figure 4 | Morphology and performance characterization of laser written micro-supercapacitors. a, Photograph of an array of concentric circular patterns fabricated on a free-standing hydrated GO film. **b**, SEM image of the interface between GO and RGO (scale bar, 100 μm), with yellow arrows indicating a long-range pseudo-ordered structure generated by laser-beam scanning. **c**, Long cyclability tests of the as-prepared sandwich and concentric circular devices, showing a less than 35% drop in capacitance after 10,000 cycles. **d**, Histogram comparison of area-based capacitance density of a sandwich device as-prepared (dark yellow), with excess DI water (navy), aqueous electrolyte (1.0 M Na_2SO_4, purple) and organic electrolyte (1.0 M $TEABF_4$, burgundy). Inset: volumetric energy density versus power density data of the corresponding devices (shown in the same colours). Error bars represent the standard error of the mean of five independent experiments.

impurities and heteroatoms remaining in the RGO. Self-discharge data for a concentric circular device are also presented in Supplementary Fig. S9, and show ~80% voltage retention within the first half hour and ~50% retention over a period of 8 h.

When an extra drop of deionized (DI) water was added into the as-prepared device, ion transport was enhanced, showing a threefold increase in capacitance (Fig. 4d). In the presence of external electrolytes, the performances of the devices were further improved. The capacitive behaviour with external aqueous (1.0 M Na_2SO_4) and organic (1.0 M $TEABF_4$ in acetonitrile) electrolytes was characterized, and results for the sandwich device are shown in Fig. 4d (Supplementary Fig. S10).

We have successfully demonstrated the ionic conductivity and use of as-prepared hydrated GO films as a new type of separator/electrolyte membrane system. The ability to reduce and pattern hydrated GO films using laser irradiation has enabled the development of a scalable process to write micro-supercapacitors on these films, which work with or without the use of external electrolytes. Our unique method is very different from the printing processes typically used in building micro-supercapacitors, but there is scope for the two to be used in a complementary fashion. Also, GO films offer an entirely different type of porous solid electrolyte and could find applications as lightweight membranes in various energy storage applications.

Methods

GO was prepared as reported in the literature[7]. Free-standing GO films were made by vacuum filtration (see Supplementary Information for details), and used directly for X-ray photoelectron spectroscopy (XPS, PHI Quantera) and XRD (Rigaku/D, CuKα radiation) characterizations. Laser reduction was conducted with a CO_2 laser printer (Universal X-660 Laser Cutter Platform; power, 2.4 W; scanning speed, 30%). Sheet resistivity was measured using a four-point probe resistivity meter (Jandel RM3) with a fixed current of 1 μA in a clean room. Scanning electron microscopy (SEM) images of the as-prepared device were obtained on a high-resolution field-emission scanning electron microscope (FEI Quanta 400). Conductive polyvinyl tapes and carbon-coated aluminium foils (Exopack Advanced Coatings) were used as current collectors.

CV, galvanostatic charge-discharge (GAL) and electrochemical impedance spectroscopy (EIS) measurements were used to characterize supercapacitor performance using an Autolab workstation (PGSTAT302N). The aqueous electrolyte was 1.0 M Na_2SO_4 (ACS grade) and the organic electrolyte was 1.0 M tetraethylammonium tetrafluoroborate ($TEABF_4$, electrochemical grade, >99%, Sigma Aldrich) in anhydrous acetonitrile (99.8%, Sigma Aldrich). Devices in organic electrolyte were assembled in argon atmosphere in a dry glovebox. The ionic conductivity of the pristine GO was determined from complex impedance spectra measured using the Autolab (PGSTST302N) with a frequency ranging from 1 MHz to 100 Hz. A conductivity cell containing two stainless-steel blocking electrodes with an intact GO film was used for this measurement[20]. Silver was sputter-coated onto both surfaces of the GO film to improve the contact. Parameters and calculations are discussed in detail in the Supplementary Information.

Received 26 April 2011; accepted 14 June 2011; published online 31 July 2011

References

1. Chmiola, J., Largeot, C., Taberna, P. L., Simon, P. & Gogotsi, Y. Monolithic carbide-derived carbon films for micro-supercapacitors. *Science* **328,** 480–483 (2010).
2. Pech, D. *et al.* Elaboration of a microstructured inkjet-printed carbon electrochemical capacitor. *J. Power Sources* **195,** 1266–1269 (2010).
3. Pech, D. *et al.* Ultrahigh-power micrometre-sized supercapacitors based on onion-like carbon. *Nature Nanotech.* **5,** 651–654 (2010).

© 2011 Macmillan Publishers Limited. All rights reserved.

4. Liu, X. J. & Osaka, T. All-solid-state electric double-layer capacitor with isotropic high-density graphite electrode and polyethylene oxide/$LiClO_4$ polymer electrolyte. *J. Electrochem. Soc.* **143,** 3982–3986 (1996).
5. Rikukawa, M. & Sanui, K. Proton-conducting polymer electrolyte membranes based on hydrocarbon polymers. *Prog. Polym. Sci.* **25,** 1463–1502 (2000).
6. Hummers, W. S. & Offeman, R. E. Preparation of graphitic oxide. *J. Am. Chem. Soc.* **80,** 1339 (1958).
7. Gilje, S., Han, S., Wang, M., Wang, K. L. & Kaner, R. B. A chemical route to graphene for device applications. *Nano Lett.* **7,** 3394–3398 (2007).
8. Gao, W., Alemany, L. B., Ci, L. J. & Ajayan, P. M. New insights into the structure and reduction of graphite oxide. *Nature Chem.* **1,** 403–408 (2009).
9. Cerveny, S., Barroso-Bujans, F., Alegria, A. & Colmenero, J. Dynamics of water intercalated in graphite oxide. *J. Phys. Chem. C* **114,** 2604–2612 (2010).
10. Thampan, T., Malhotra, S., Tang, H. & Datta, R. Modeling of conductive transport in proton-exchange membranes for fuel cells. *J. Electrochem. Soc.* **147,** 3242–3250 (2000).
11. Park, K. W., Ahn, H. J. & Sung, Y. E. All-solid-state supercapacitor using a Nafion® polymer membrane and its hybridization with a direct methanol fuel cell. *J. Power Sources* **109,** 500–506 (2002).
12. Eda, G., Fanchini, G. & Chhowalla, M. Large-area ultrathin films of reduced graphene oxide as a transparent and flexible electronic material. *Nature Nanotech.* **3,** 270–274 (2008).
13. Tung, V. C., Allen, M. J., Yang, Y. & Kaner, R. B. High-throughput solution processing of large-scale graphene. *Nature Nanotech.* **4,** 25–29 (2009).
14. Eda, G. & Chhowalla, M. Chemically derived graphene oxide: towards large-area thin-film electronics and optoelectronics. *Adv. Mater.* **22,** 2392–2415 (2010).
15. Cai, W. W. *et al.* Synthesis and solid-state NMR structural characterization of ^{13}C-labeled graphite oxide. *Science* **321,** 1815–1817 (2008).
16. Casablanca, L. B. *et al.* NMR-based structural modeling of graphite oxide using multidimensional ^{13}C solid-state NMR and *ab initio* chemical shift calculations. *J. Am. Chem. Soc.* **132,** 5672–5676 (2010).
17. Park, S. *et al.* Aqueous suspension and characterization of chemically modified graphene sheets. *Chem. Mater.* **20,** 6592–6594 (2008).
18. Wei, Z. *et al.* Nanoscale tunable reduction of graphene oxide for graphene electronics. *Science* **328,** 1373–1375 (2010).
19. Zhang, Y. L. *et al.* Direct imprinting of microcircuits on graphene oxides film by femtosecond laser reduction. *Nano Today* **5,** 15–20 (2009).
20. Abraham, K. M., Jiang, Z. & Carroll, B. Highly conductive PEO-like polymer electrolytes. *Chem. Mater.* **9,** 1978–1988 (1997).
21. Hirata, M., Gotou, T. & Ohba, M. Thin-film particles of graphite oxide. 2: Preliminary studies for internal micro fabrication of single particle and carbonaceous electronic circuits. *Carbon* **43,** 503–510 (2005).
22. Petit, C., Seredych, M. & Bandosz, T. J. Revisiting the chemistry of graphite oxides and its effect on ammonia adsorption. *J. Mater. Chem.* **19,** 9176–9185 (2009).
23. Agmon, N. The Grotthuss mechanism. *Chem. Phys. Lett.* **244,** 456–462 (1995).
24. Saito, M., Arimura, N., Hayamizu, K. & Okada, T. Mechanisms of ion and water transport in perfluorosulfonated ionomer membranes for fuel cells. *J. Phys. Chem. B* **108,** 16064–16070 (2004).
25. Mauritz, K. A. & Moore, R. B. State of understanding of Nafion. *Chem. Rev.* **104,** 4535–4585 (2004).
26. Punckt, C., Pope, M. A., Liu, J., Lin, Y. & Aksay, L. A. Electrochemical performance of graphene as effected by electrode porosity and graphene functionalization. *Electroanalysis* **22,** 2834–2841 (2010).
27. Taberna, P. L., Portet, C. & Simon, P. Electrode surface treatment and electrochemical impedance spectroscopy study on carbon/carbon supercapacitors. *Appl. Phys. A* **82,** 639–646 (2006).
28. Balducci, A. *et al.* Cycling stability of a hybrid activated carbon/poly(3-methylthiophene) supercapacitor with *N*-butyl-*N*-methylpyrrolidinium bis(trifluoromethanesulfonyl)imide ionic liquid as electrolyte. *Electrochim. Acta* **50,** 2233–2237 (2005).
29. Chen, Y., Zhang, X., Zhang, D., Yu, P. & Ma, Y. High performance supercapacitors based on reduced graphene oxide in aqueous and ionic liquid electrolytes. *Carbon* **49,** 573–580 (2011).
30. Stoller, M. D., Park, S. J., Zhu, Y. W., An, J. H. & Ruoff, R. S. Graphene-based ultracapacitors. *Nano Lett.* **8,** 3498–3502 (2008).

Acknowledgements

W.G. and P.M.A. acknowledge funding support from Nanoholdings, LLC. The authors also thank B. Pradhan for discussions.

Author contributions

W.G. prepared the GO, fabricated devices and collected characterization data. A.L.M.R., N.S. and W.G. conducted ionic conductivity testing and data analysis. Z.L., L.S. and W.G. conducted conductivity measurements and analysed the data. L.C. and R.V. were involved in study design. P.M.A., W.G. and L.C. designed the study. P.M.A., W.G. and N.S. wrote the paper. Q.Z. and B.W. conducted self-discharge measurements and analysed the relevant data. All authors discussed the results and commented on the manuscript.

Additional information

The authors declare no competing financial interests. Supplementary information accompanies this paper at www.nature.com/naturenanotechnology. Reprints and permission information is available online at http://www.nature.com/reprints. Correspondence and requests for materials should be addressed to P.M.A.

© 2011 Macmillan Publishers Limited. All rights reserved.